Steel and Composite Structures, Vol. 10, No. 4 (2010) 317-329
DOI: http://dx.doi.org/10.12989/scs.2010.10.4.317

Study on push-out test and bond stress-slip relationship of circular concrete filled steel tube

Yin Xiaowei* and Lu Xilin

State Key Laboratory of Disaster Reduction in Civil Engineering, Tongji University, Shanghai 200092, China

(Received September 16, 2009, Accepted June 16, 2010)

Abstract. According to the results of 9 circular concrete filled steel tube (CFT) push-out tests, a new theoretical model for average bond stress versus free end slip curve is proposed. The relationship between average bond stress and free end slip is obtained considering some varying influential parameters such as slenderness ratio and diameter-to-thickness ratio. Based on measured steel tube strain and relative slip at different longitudinal positions, the distribution of bond stress and relative slip along the length of steel tube is obtained. An equation for predicting the varying bond-slip relationship along longitudinal length and a position function reflecting the variation are proposed. The presented method can be used in the application of finite element method to analyze the behavior of CFT structures.

Keywords: concrete filled steel tube; bond-slip; push-out test; constitutive relationship; position function.

1. Introduction

In concrete-filled steel tube (CFT) structures, one of the behavioral problems is the bond between concrete and steel tube and, in fact, whether the system concrete-steel tube could work in cooperation depends greatly on the transfer mechanisms at the interface. Similar to concrete structures, bond stress could be seen as shear stress between the steel tube and concrete. Due to the bond stress, partial applied load transfers from steel tube to concrete, hence the two materials could work in cooperation. In the last decade several research works were carried out to investigate the bond between steel tube and concrete, whereas some problems still need further studies in order to obtain reliable design indications. In addition, while finite element method is conducted, reliable bond-slip constitutive relationship of CFTs must be taken into account to develop reliable numerical models. However, the relative slip between the steel tube and concrete is hard to examine, while the traditional way is to assume the relationship between average stress and the slip of loaded or free end as the real constitutive relationship of CFTs. In fact, the distribution of bond stress is not uniform along the longitudinal length.

Therefore, it is necessary to carry out further study on the bond-slip performance between the steel tube and the concrete experimentally and theoretically. In this paper, 9 push-out tests on circular CFTs with different slenderness ratios and diameter-to-thickness ratios are reported, and also the slips at free end are measured respectively. The relationship of average bond stress-free end slip is addressed in this paper.

In order to obtain the local bond stress-slip relationships of the steel tube–concrete interface directly

* Corresponding author, Ms., E-mail: yxwtoo567@163.com

from the push-out test, a series of strain gauges were attached with small intervals on the surface of steel tube. As a result, the strain distributions of steel tube along the longitudinal interface corresponding to each load level were obtained. Additionally, 4 steel sticks were embedded in the concrete through the slots which were reserved along the steel tube with uniform intervals while one of them was intentionally located close to the free end. 4 displacement transducers were set correspondingly between the steel tube and the non-embedded ends of the steel sticks. In this way, when the concrete slipped under the applied load, the embedded steel sticks moved with the concrete. The slips recorded by displacement transducers were the real relative slip of CFTs at different longitudinal positions. Based on the measured data, the varying bond-slip constitutive relationship along longitudinal length was obtained, and a position function reflecting the variation is deduced. At the end of this paper, local bond-slip relationship considering longitudinal position is proposed.

2. Experimental investigation

The experimental investigation includes 9 circular CFT push-out members with different slenderness ratios (4L/D) and diameter-to-thickness ratios (D/t). The characteristics of tested specimens are presented in Table 1.

The steel used in these tests was Q235, and the steel tubes were straight welded. Commercial concrete was utilized. The mechanical proprieties of the concrete were experimentally estimated: the average compressive strength was about 58.57 MPa, and the average tensile strength was 3.92 MPa.

The details of the experimental setup are shown in Fig. 1(a). In order to exert uniform compressive forces to the specimens, one square thick steel plate was adhered to the free end of each CFT member, while the circular one was adhered to the loaded end, and the diameter of the circular steel plate was slightly less than the inner diameter of the specimen. In Fig. 1(a), a gap is left at the free end between the concrete and the loading plate. By loading only on the steel tube at the top of the specimen and supporting only in the concrete at the bottom, all applied loads will be transferred through the steel-concrete interface.

During the push-out test procedures, the displacement control loading system was applied, and a 500-ton compression machine was used. One displacement transducer was set at the loaded end and 4 were set to measure the local relative slips between the embedded steel sticks and the steel tube. Load cells and transducers were connected to the data logger then the load and slip signals were recorded simultaneously by a computer.

According to the length of the specimens, strain gauges were bonded to the outside surface of steel tubes with interval of 30 mm or 40 mm. During the manufacturing process of the steel tube, 4

Table 1 Characteristics of CFTs

CFT	Steel tube type	Length (L)/mm	Slenderness ratio (4L/D)	Diameter-to-thickness ratio(D/t)	Outer diameter (D)/mm	Thickness (t)/mm
TCA-1	Φ159 × 4	500	12.58	39.75	159	4
TCA-2	Φ159 × 4	700	17.61	39.75	159	4
TCA-3	Φ159 × 4	900	22.64	39.75	159	4
TCB-1	Φ159 × 4.5	500	12.58	35.33	159	4.5
TCB-2	Φ159 × 4.5	700	17.61	35.33	159	4.5
TCB-3	Φ159 × 4.5	900	22.64	35.33	159	4.5
TCC-1	Φ159 × 5.5	500	12.58	28.91	159	5.5
TCC-2	Φ159 × 5.5	700	17.61	28.91	159	5.5
TCC-3	Φ159 × 5.5	900	22.64	28.91	159	5.5

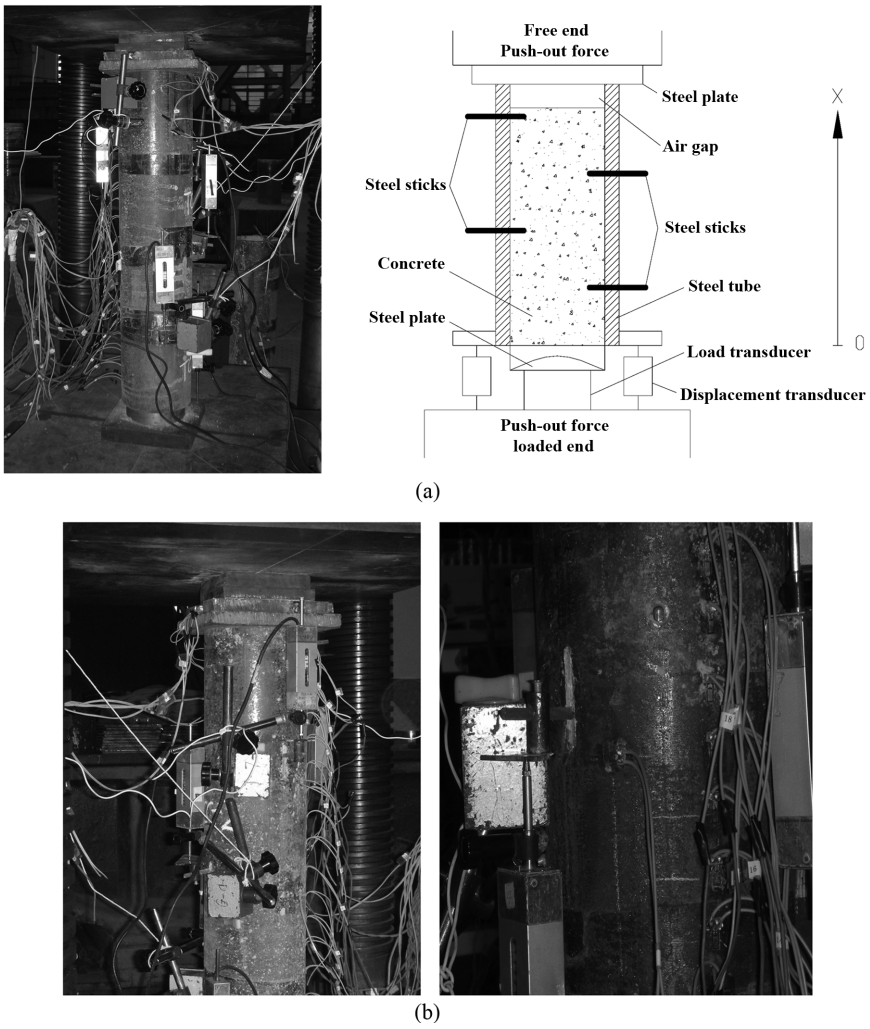

Fig. 1(a) Test setup-standard push-out test, (b) Details of the displacement transducers at the free end and the slots of the steel tube

longitudinal slots were reserved with uniform distance along the longitudinal surface, and when the concrete was cast, 4 steel sticks were fixed into the concrete through those slots. In particular, one of them was fixed near the top of the concrete, and the free end slip could be measured there. The length of the slots was 50 mm, and the diameter of the steel sticks was 4 mm. The details of displacement transducers and slots of the steel tube are shown in Fig. 1(b).

3. Average bond stress-free end slip ($\overline{\tau}-s_j$)

3.1 Average bond stress-free end slip curve

In push-out tests, applied loads and displacement values are used to calculate the corresponding

average bond stresses and slips. The value of average bond stress is calculated as follows with the assumption of uniform bond stress distribution along the bond length.

$$\bar{\tau} = \frac{P}{\pi D_0 L} \tag{1}$$

In Eq. (1), P is the applied push-out load; D_0 is the inner diameter of steel tube; L is the length of the specimen.

The values of free end slip (s_j) were measured continuously under increasing load by one displacement transducer as indicated in Fig. 1(a).

Push-out failure is defined as the point of bond failure load (P_u). The corresponding average bond failure strength ($\bar{\tau}_u$) and slip (s_{ju}) values are then defined as those values occurring at the point of failure.

According to Eq. (1), the average bond stress-free end slip curves are obtained. Some of them are shown in Fig. 2. The figure appears that, the entire bond stress-slip curves present 3 stages: the non-slip stage, ascending stage, and residual stage. In the non-slip stage, the bond stress continuously ascends with no slippage occurring. After a certain point, in the ascending stage, a nonlinear relationship between bond stress and the slip is identified. In this stage, the bond stress increases significantly with a corresponding increase in slip until the bond failure strength ($\bar{\tau}_u$) is reached. The load transfer from steel tube to concrete in this phase depends mainly on adhesion and mechanical interlock, and the mechanical properties and surface condition of steel tubes can strongly influence their push-out behavior. In the residual stage, CFT specimens exhibit a sharp increase in relative slip with nearly no

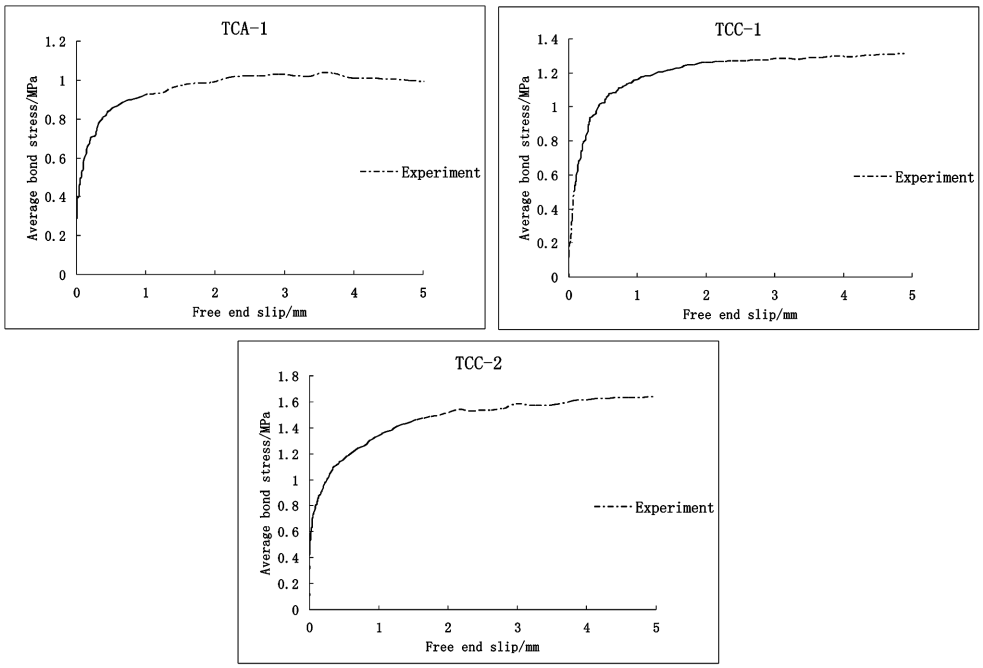

Fig. 2 Average bond stress versus free end slip curves of typical specimens

increase under push-out load. This implies that the residual push-out load depends only on the friction resistance, and the mechanical interlock between the steel tube and concrete has failed.

Theoretical model of the average bond stress-free end slip is shown in Fig. 3. In this model, non-slip stage (OA section) is simplified as one vertical line, while the residual stage (BC section) is simplified as one horizontal line.

According to the discussion above, the average bond stress-free end slip model of CFTs could be uniquely determined by two key points, and the two points could be defined as follows:

1) The initial slipping point (0, $\bar{\tau}_s$), where $\bar{\tau}_s$ is the initial slipping strength, corresponding to the initial slip, and is defined as $\bar{\tau}_s = \dfrac{P_s}{\pi D_0 L}$, where P_s is the applied load under which the initial slip occurred.

2) The bond failure point(s_{ju}, $\bar{\tau}_u$) where $\bar{\tau}_u$ is bond failure strength, and is defined as $\bar{\tau}_u = \dfrac{P_s}{\pi D_0 L}$; s_{ju} is the corresponding slip value; P_u is the bond failure load, corresponding to the beginning point of flat tail in the average bond stress versus free end slip curve.

3.2 Two key points of the average bond stress versus free end slip curve

The regression equations of the coordinate values of bond failure point (s_{ju}, $\bar{\tau}_u$) of the average bond stress-free end slip curve mentioned above are suggested by considering the influences of the slenderness ratio (4L/D), diameter to thickness ratio (D/t), tensile strength of the concrete(f_t) as well as the surface condition. The equations can be expressed as given below

$$\bar{\tau}_u = \frac{1}{\gamma}k\left[1226.3334 + 69.4376\times\left(\frac{4L}{D}\right) - 2.075\times\left(\frac{4L}{D}\right)^2 - 80.2587\times\left(\frac{D}{t}\right) + 1.0614\times\left(\frac{D}{t}\right)^2\right] f_t/1000 \quad (2a)$$

$$s_{ju} = \frac{1}{\gamma}k\left[-22.7756 + 1.1264\times\left(\frac{4L}{D}\right) - 0.0308\times\left(\frac{4L}{D}\right)^2 + 0.9464\left(\frac{D}{t}\right) - 0.0142\times\left(\frac{D}{t}\right)^2\right] \quad (2b)$$

While the ordinate value of the initial slipping point is proposed as $0.3\bar{\tau}_u$, namely

$$\bar{\tau}_s = 0.3\bar{\tau}_u \quad (3)$$

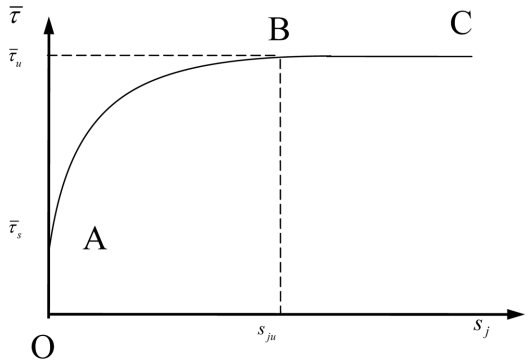

Fig. 3 Theoretical model for average bond stress versus free end slip curve

In above equations, γ is the correction factor reflecting the uncertainties during the test, and in this paper, it is proposed to be 0.98; k is the influential factor of the surface condition. According to the study of Xu (1990), k equals to 1.0 when the rust in the inner surface of the steel tube is cleaned by manual.

The average bond stress-free end slip curves of the 9 CFT specimens are different. In order to develop a unified analytical model, the relative steady values: bond failure strength $\bar{\tau}_u$ and its corresponding slip are s_{ju} introduced as the basic values of the skeleton curve to unify the skeleton curves (Fig. 4). The curves shown in Fig. 4 agree with the analytical curve shown in Fig. 3. Therefore, in this paper the average bond stress-free end slip curve is developed by using the values: bond failure strength $\bar{\tau}_u$, and its corresponding slip s_{ju}.

The average bond stress-free end slip curve can be expressed as given below

$$\bar{\tau}(s_j) = \begin{cases} s_j = 0 & 0 < \bar{\tau} \le \bar{\tau}_s \\ \dfrac{(s_j/s_{ju})}{0.1 + 1.22 \times (s_j/s_{ju}) + 0.11 \times \sqrt{(s_j/s_{ju})}} + 0.28 & 0 < s_j \le s_{ju} \\ \bar{\tau} = \bar{\tau}_u & s_{ju} < s_j \end{cases} \times \bar{\tau}_u \tag{4}$$

Substituting Eq. (2) and Eq. (3) into Eq. (4), the calculated curves are obtained. The comparisons between the analytical curves and the experimental ones are shown in Fig. 5. It can be seen that good agreement are reached.

4. Bond stress and relative slip

4.1 Longitudinal stress distribution of steel tube along the length (σ_S–x)

Fig. 6 illustrates the typical longitudinal stress distribution curves of steel tubes. In Fig. 6 where X denotes the distance from the loaded end to the measuring point, the stresses of steel tubes increase rapidly in the loaded and free ends, while in the cross sections away from the two ends the stresses

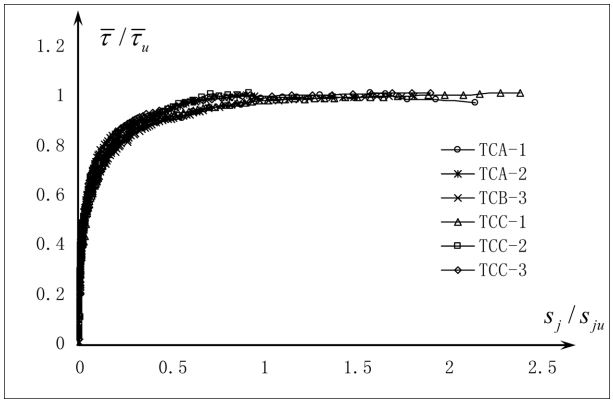

Fig. 4 The dimensionless curves of average bond stress versus free end slip

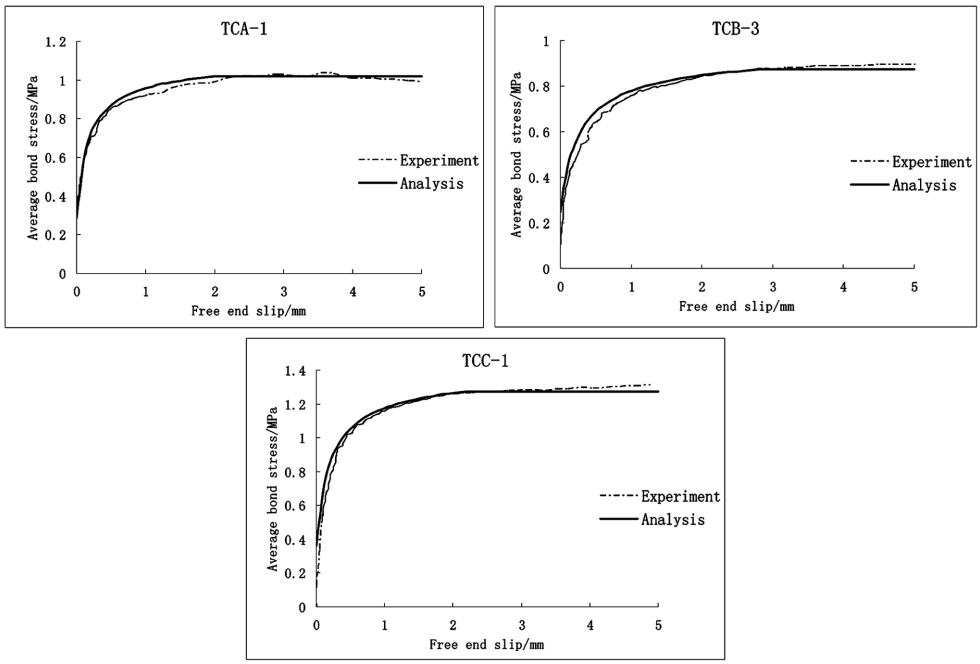

Fig. 5 Comparison of average bond stress versus free end slip for experiment cases and analysis cases

increase slowly. At the beginning of loading, the distribution is nearly horizontal, and with the increase of loading, the entire curve turns to be a cubic curve.

4.2 Distribution of bond stress

Due to the dense arrangement of strain gauges along the length of the specimens, if the subsequent discussion according to traditional analytical method: firstly calculate the stress difference of two adjacent sections, secondly delineate the trend of bond stress curve by smooth curves, the bond stress curves will be rather disordered. Therefore, according to the shape of stress curve for steel tube, cubic curve model is used to simulate the curves. Since the bond stress was proportional to the differential of strain of steel tube, differentiating the stress curves, the distribution law of bond stress is obtained. In addition, the numerical integration of bond stress curves under different loading levels is conducted, and the result should be equal to the value of applied load. If any exception exists, the difference between applied load and the integration sum of bond stress curve should be evenly distribute to each measuring point along the steel tube, and the area enveloped by the adjusted bond stress curve will be equal to the applied load. Then the distribution laws of bond stress along the longitudinal length of steel tubes are obtained. Typical bond stress distributions along the longitudinal length of different loading levels are displayed in Fig. 7.

According to the equilibrium condition, the bond stresses of the two ends are zero, whereas the strains of steel tube and concrete core are maximal at the two ends respectively. Combining with the effect of boundary condition, some singularity phenomena of bond stress and strain would appear in a limited region close to the ends. Fortunately, the distribution of the stress is not affected in other regions. Therefore, in this paper the regions which are 0.1 L away from the two ends are defined as local bond stiffness increasing regions, that is to say, the maximal bond stresses under different loading levels

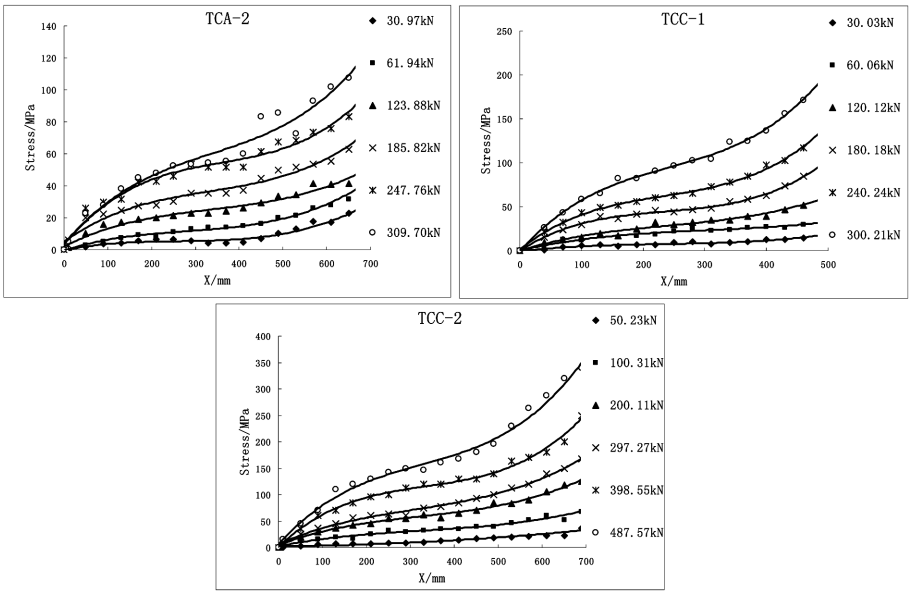

Fig. 6 Stress curves of steel tube for typical specimens

appear in the points which are 0.1 L away from the two ends, as can be seen in Fig.7. The distributions of bond stress and strain in the local bond stiffness increasing regions are not mentioned in this paper, and further research will be conducted in the future study.

4.3 Distribution of relative slip

For the purpose of practical requirement, 4 steel sticks were inserted into the concrete core through slots of steel tubes. In this way, the local slip of steel tube to concrete along the longitudinal length could be directly measured by displacement transducers, and the toughest problem of bond slip experimental research is consequently solved. Slip curves of typical specimens under different loading levels are illustrated in Fig. 8.

In Fig. 8, at the beginning of loading, slippage appears in the loaded end. As load increases, in some specimens (such as TCB-2), the slips in the loaded and free ends increase rapidly, while the slips in the two ends are larger than the slips in other sections. But for the majority of specimens (such as TCC-2), the slip in loaded end is distinctly larger than any other sections, while the free end has an equal slip with those sections far from the two ends. Specimen TCA-2 is an exception, the slip in the free end of this specimen is smaller than other sections under any load levels.

5. Local bond-slip constitutive relationship

5.1 Bond-slip constitutive relationship of different positions

According to Fig. 7 and Fig. 8, bond-slip constitutive relationships of different positions can be obtained (Fig. 9). Based on the characteristic of the shape of curves shown in Fig. 9, a reasonable

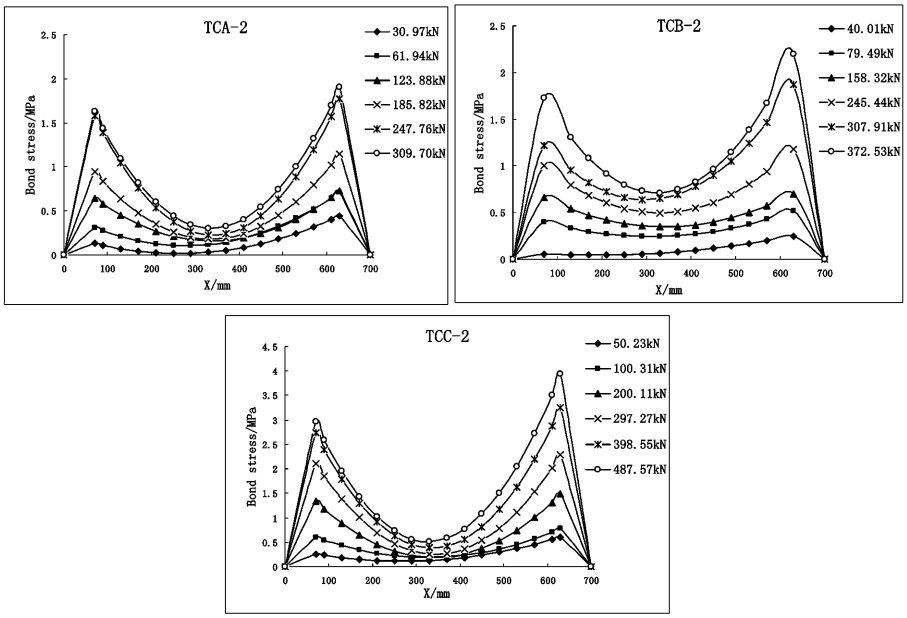

Fig. 7 Typical bond stress distribution under different loading levels

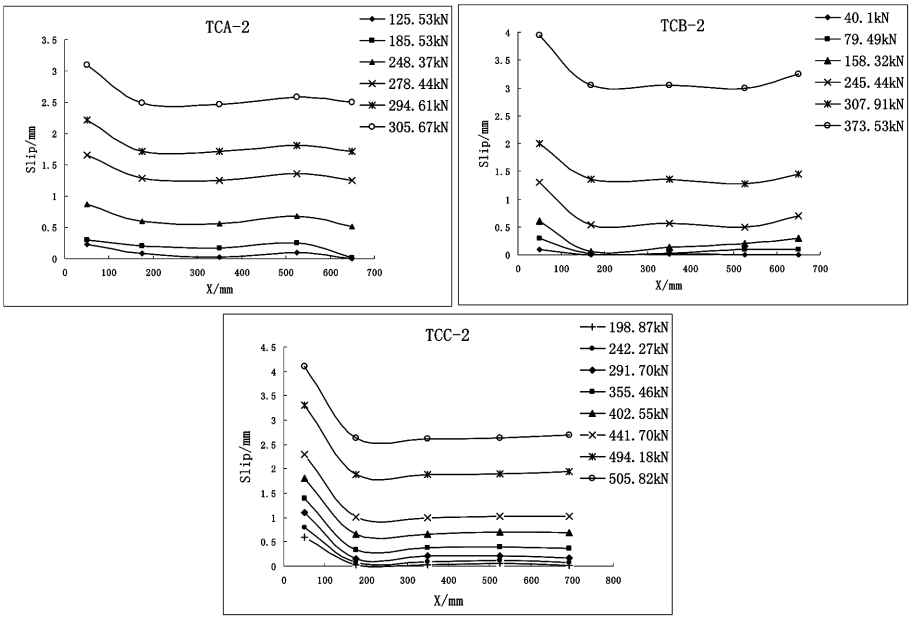

Fig. 8 Typical relative slip curves under different loading levels

assumption could be proposed: the bond-slip curves of different positions share the same shape with the theoretical model of average bond stress-free end slip relationship which is shown in Fig. 3, and the local bond-slip ($\tau(x)-s(x)$) curve could be described as the product of a basic bond-slip relationship

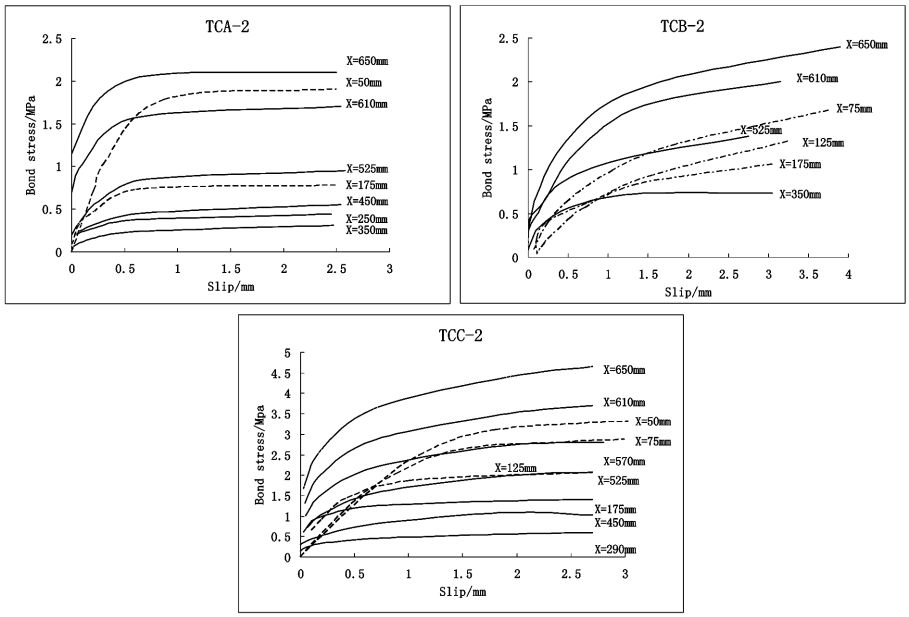

Fig. 9 Bond stress versus slip relationship of different longitudinal positions

$\phi(s)$ and a position function $\psi(x)$. Generally, the average bond stress-free end slip ($\overline{\tau}-s_j$) relationship could act as the basic relationship. Therefore, the local bond-slip constitutive relationship of circular CFTs can be described as follows

$$\tau(s,x) = \phi(s) \cdot \psi(x) \tag{5}$$

In Eq. (5), $\tau(s,x)$ is the bond-slip constitutive relationship of different longitudinal positions; s is the local slip; $\phi(s)$ is the basic bond-slip relationship according to Eq. (4); $\psi(x)$ is the position function according to Eq.(6).

5.2 Position function

The position function reveals relative bond stiffness of different positions. It can be obtained by the following method: draw the family of bond stress curves for different positions under different slip levels, divide the ordinate $\tau(x)$ by average bond stress ($\overline{\tau}$) under the same slip level, and divide the abscissa x by specimen length L, then the dimensionless curve whose mean ordinate value is 1 is obtained. This curve is the bond-slip position function $\psi(x)$, and the solution procedure is presented in Fig. 10. Typical position function curves of the specimens are shown in Fig. 11 (a).

In order to simplify the analysis, the position function curves of all the 9 specimens are presented in Fig. 11 (b), neglecting the influence of local bond stiffness increasing regions closed to the two ends. The position function of circular CFT push-out specimens can be described by two straight-lines and one second-degree parabola, as is expressed in Eq. (6). The function proposed in Eq. (6) is also shown in Fig. 11(b).

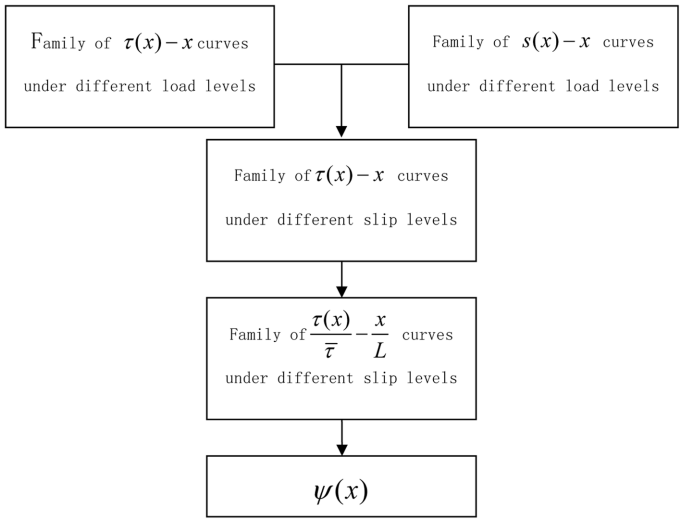

Fig. 10 Solution procedure of the position function

$$\psi(x)=\begin{cases} 18.0005\left(\frac{x}{L}\right) & 0\le\left(\frac{x}{L}\right)<0.1 \\ 10.375\left(\frac{x}{L}\right)^2-9.625\left(\frac{x}{L}\right)+2.6588 & 0.1\le\left(\frac{x}{L}\right)\le 0.9 \\ -24.0005\left(\frac{x}{L}\right)+24.0005 & 0.9<\left(\frac{x}{L}\right)\le 1 \end{cases} \tag{6}$$

Therefore, replacing notation s_j in Eq. (4) by local slip notation s, and replacing $\bar{\tau}(s_j)$ by $\phi(s)$, substituting this new relationship and Eq. (6) into Eq. (5), the varying bond-slip relationship along longitudinal length of circular CFT members is obtained.

6. Conclusions

In order to study the local bond behavior of circular CFTs, 9 push-out tests were carried out. Mathematical representations of two key points in average bond stress-free end slip curve are suggested. Utilizing the two key points, average bond stress-free end slip curves of CFTs members with different lengths, thicknesses of the steel tube, outer diameters and concrete strength could be uniquely determined according to Eq. (4). However, average bond stress-free end slip curve is not able to truly represent the actual relationship of local bond stress-slip because the relationship varies with position. Based on this, local slips were measured in the test, and bond stress distribution is calculated by differentiating the stress curve of steel tube along the length. A family of bond stress-slip curves for different positions is obtained. Since the shape of all the local bond stress-slip curves is similar to their own average bond stress-free end slip, a position function which could reflect the relationship between

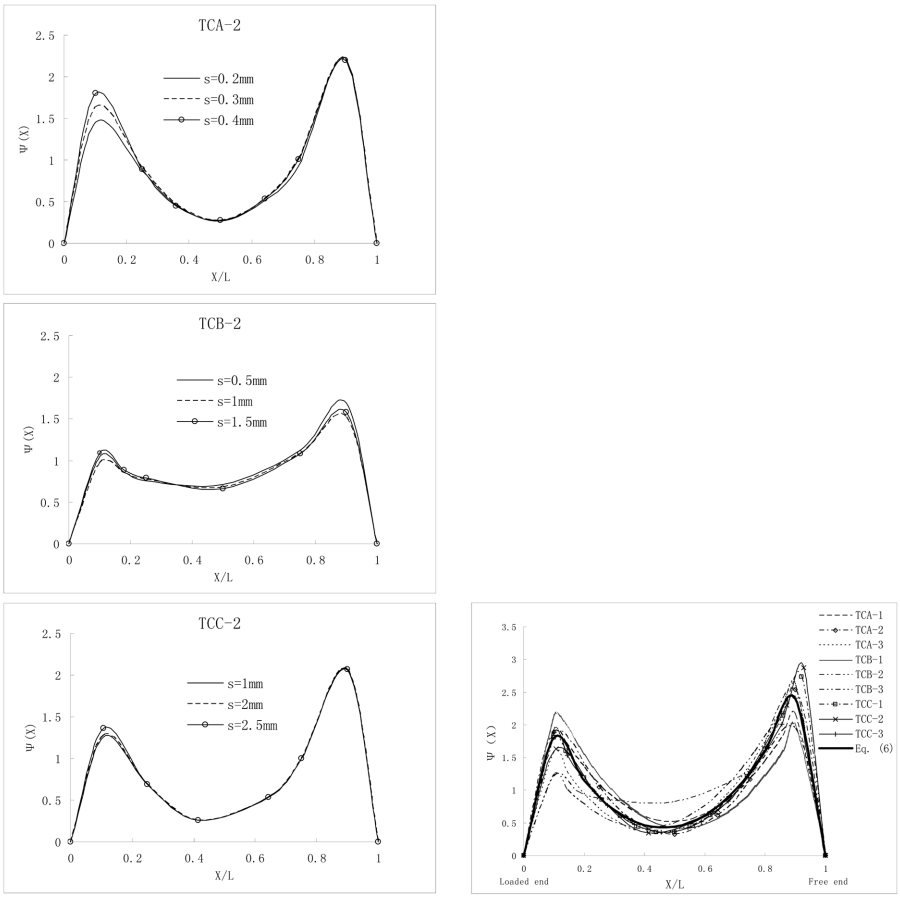

(a) (b)

Fig. 11 (a) Position functions of typical specimens, (b) Position functions of all the 9 specimens

them is introduced, and the relationship of bond stress-slip in every position could be derived from Eq.(5). The equation of position function is proposed in Eq. (6).

In practical application, substituting the parameters of the specimens such as the length, thickness of the steel tube, outer diameter and concrete strength into Eq. (2), the coordinates of the two key points $(0, \overline{\tau}_s)$ and $(s_{ju}, \overline{\tau}_u)$ are obtained, and the basic bond-slip relationship $\phi(s)$ is determined. Deriving the function $\psi(x_0)$ in any position from Eq. (6), substituting $\phi(s)$ and $\psi(x_0)$ in to Eq. (5), one can get the local bond stress-slip relationship in any position of CFT members.

It is worth noted that all the equations proposed in this study can only apply to CFTs members using Q235 steel and concrete with a compressive strength of 58.57 MPa. The model cannot be used as a general one until it has been validated by comparisons with other experimental results. Similar research can be conducted on CFT members using the method mentioned in this paper, and the presented model can be utilized in the application of finite element analysis to study the behavior of certain CFT structures.

7. Acknowledgements

The authors are grateful for the partial financial support by National Natural Science Foundation of China through grant 90815029 and grant 51021140006.

References

Achillides, Z. and Pilakoutas, K. (2004), "Bond behavior of fiber reinforced polymer bars under direct pullout conditions", *J. Compos. Constr.*, **8**(2), 173-181.

Aiello, M.A., Leone, M. and Pecce, M. (2007), "Bond performances of FRP rebars-reinforced concrete", *J. Mater. Civil. Eng.*, **19**(3), 205-213.

Almusallam, A.A., Al-Gahtani, A.S. and Rasheeduzzafar, A.R. (1996), "Effect of reinforcement corrosion and cracking on bond strength", *Constr. Build. Mater.*, **10**(2),123-129.

Al-Sulaimani, G.J., Kaleemullah, M., Basunbul, I.A. and Rasheeduzzafar, A.R. (1990), "Influence of corrosion and cracking on bond behavior and strength of reinforced concrete members", *ACI Struct. J.*, **87**(2), 220-231.

Dai, J.G., Ueda, T. and Sato, Y. (2005), "Development of the nonlinear bond stress-slip model of fiber reinforced plastics sheet-concrete interfaces with a simple method", *J. Compos. Constr.,* **9**(1), 52-62.

Hajjar, J.F. and Gourley, B.C. (1996), "Representation of concrete-filled steel tube cross-section strength", *J. Struct. Eng-ASCE*, **122**(11), 1327-1336.

Lee, H.S., Noguchi, T. and Tomosawa, F. (2002), "Evaluation of the bond properties between concrete and reinforcement as a function of the degree of reinforcement corrosion", *Cement. Concrete. Res.*, **32**(8), 1313-1318.

Lu, X.L. (2007), *Seismic theory and application for complex high-rise structures*, Science Press, China.

Mains, R.M. (1951), "Measurement of the distribution of tensile and bond stresses along reinforcing bars", *ACI J.,* **48**(11), 225-252.

Malvar, L.J. (1995), "Tensile and bond properties of GFRP reinforcing bars", *ACI Mater. J.*, **92**(3), 276-285.

Okelo, R. and Yuan, R.L. (2005), "Bond strength of fiber reinforced polymer rebars in normal strength concrete", *J. Compos. Constr.*, **9**(3), 203-213.

Roeder, C.W., Chmielowski, R. and Brown C.B. (1999), "Shear connector requirements for embedded steel sections", *J. Struct. Eng-ASCE*, **125**(2), 142-151.

Schiller, P.H., Hajjar, J.F. and Molodan, A. (1998), "A distributed plasticity formulation for three-dimensional rectangular concrete-filled steel tube beam columns and composite frames", **96**(5), Dept. of Civ. Eng. Univ. of Minneapolis, Minneapolis.

Shakir-Khalil, H. (1993), "Push out strength of concrete-filled steel hollow sections", *Struct. Eng.*, **71**(13), 230-233.

Shakir-Khalil, H. and Zeghiche, Z. (1989), "Experimental behavior of concrete-filled rolled rectangular hollow section columns", *Struct. Eng.*, **67**(19), 345-353.

Somayaji, S. and Shah, S.P. (1981), "Bond stress versus slip relationship and cracking response of tension members", *ACI J.*, **78**(3), 217-224.

Tassios, T.P. and Yannopulos, P.J. (1981), "Analytical studies on reinforced concrete members under cyclic loading based on bond stress-slip relationships", *ACI J.*, **78**(3), 206-216.

Tastani1, S.P. and Pantazopoulou, S.J. (2006), "Bond of GFRP bars in concrete: experimental study and analytical interpretation", *J. Compos. Constr.*, **10**(5), 381-391.

Xu, Y.L. (1990), *Experimental study of bond-anchorage properties for deformed bars in concrete*, Tsinghua Univ, China.

Xue, J.Y., Yang, Y. and Zhao, H.T. (2005), "Experimental study on bond strengths of steel reinforced concrete structure", *J. Xi'an Univ. of Arch. & Tech. (Natural Science Edition)*, **37**(2), 149-154.

Zhang, B. and Benmokrane, B. (2002), "Pullout bond properties of fiber-reinforced polymer tendons to grout", *J. Mater. Civil. Eng.*, **14**(5), 399-408.

CC